Activity of Adagrasib (MRTX849) in Brain Metastases: Preclinical Models and Clinical Data from Patients with KRAS^{G12C}-Mutant Non–Small Cell Lung Cancer

Joshua K. Sabari[1], Vamsidhar Velcheti[1], Kazuhide Shimizu[2,3], Matthew R. Strickland[2,4], Rebecca S. Heist[2], Mohini Singh[2], Naema Nayyar[2], Anita Giobbie-Hurder[4], Subba R. Digumarthy[2], Justin F. Gainor[2], Anant P. Rajan[2], Edwin Nieblas-Bedolla[2], Aaron C. Burns[5], Jill Hallin[5], Peter Olson[5], James G. Christensen[5], Sylvia C. Kurz[1], Priscilla K. Brastianos[2], and Hiroaki Wakimoto[2]

ABSTRACT

Purpose: Patients with KRAS-mutant non–small cell lung cancer (NSCLC) with brain metastases (BM) have a poor prognosis. Adagrasib (MRTX849), a potent oral small-molecule KRAS^{G12C} inhibitor, irreversibly and selectively binds KRAS^{G12C}, locking it in its inactive state. Adagrasib has been optimized for favorable pharmacokinetic properties, including long half-life (∼24 hours), extensive tissue distribution, dose-dependent pharmacokinetics, and central nervous system penetration; however, BM-specific antitumor activity of KRAS^{G12C} inhibitors remains to be fully characterized.

Experimental Design: A retrospective database query identified patients with KRAS-mutant NSCLC to understand their propensity to develop BM. Preclinical studies assessed physiochemical and pharmacokinetic properties of adagrasib. Mice bearing intracranial KRAS^{G12C}-mutant NSCLC xenografts (LU99-Luc/H23-Luc/LU65-Luc) were treated with clinically relevant adagrasib doses, and levels of adagrasib in plasma, cerebrospinal fluid (CSF), and brain were determined along with antitumor activity. Preliminary clinical data were collected from 2 patients with NSCLC with untreated BM who had received adagrasib 600 mg twice daily in the phase Ib cohort of the KRYSTAL-1 trial; CSF was collected, adagrasib concentrations measured, and antitumor activity in BM evaluated.

Results: Patients with KRAS-mutant NSCLC demonstrated high propensity to develop BM (≥40%). Adagrasib penetrated into CSF and demonstrated tumor regression and extended survival in multiple preclinical BM models. In 2 patients with NSCLC and untreated BM, CSF concentrations of adagrasib measured above the target cellular IC_{50}. Both patients demonstrated corresponding BM regression, supporting potential clinical activity of adagrasib in the brain.

Conclusions: These data support further development of adagrasib in patients with KRAS^{G12C}-mutant NSCLC with untreated BM.

See related commentary by Kommalapati and Mansfield, p. 3179

Introduction

Oncogenic mutations in members of the RAS family are a common occurrence in human cancer, with alterations in KRAS accounting for 85% of these mutations (1). The highest rate of KRAS mutations are in pancreatic (∼90%), colorectal (30%–40%), and lung (∼32%) cancers (2–4). In patients with non–small cell lung cancer (NSCLC), the development of brain metastases (BM) is associated with increased morbidity and mortality (5–7). In patients with KRAS^{G12C}-mutant NSCLC, BM are detected in 27%–42% of patients at diagnosis (8–10). Although local interventions (e.g., surgical resection, whole-brain radiotherapy, and stereotactic radiosurgery) have been the cornerstone of treatment for patients with advanced NSCLC and BM, clinical outcomes remain poor, and there is an unmet need for improved, central nervous system (CNS)-penetrant pharmacologic treatment strategies in this patient population (5). Recent advances in targeted therapies, including next-generation EGFR and ALK tyrosine kinase inhibitors (TKI), suggest that CNS penetrant targeted therapies can lead to clinically meaningful activity in the CNS with improved safety profiles (11, 12). Notably, the development of brain penetrant TKIs such as osimertinib, alectinib, and lorlatinib has resulted in marked improvement in CNS clinical response and patient outcomes compared with first-generation TKIs (e.g., crizotinib, erlotinib, and gefitinib) which are thought to have more limited CNS penetration (12–15). These newer agents have cerebrospinal fluid (CSF)-to-unbound plasma ratios ($K_{p,uu}$) that indicate significant CNS penetrance (osimertinib $K_{p,uu}$ 0.39, alectinib $K_{p,uu}$ 0.63–0.94, and lorlatinib $K_{p,uu}$ 0.75), underscoring improved CNS response rates and clinical outcomes (16–18).

Historically, development of therapies targeting KRAS has proved elusive (19). However, the discovery of covalent inhibitors targeting the mutated cysteine residue in KRAS^{G12C} within the switch II binding pocket has led to the development of clinically active therapies (19–21). Recently, sotorasib became the first targeted treatment to be approved by the FDA for patients with KRAS^{G12C}-mutated locally advanced or metastatic NSCLC (22); however, the CNS penetration and activity of this agent in active and untreated BM is not yet fully characterized.

[1]Laura and Isaac Perlmutter Cancer Center, NYU Langone, New York, New York. [2]Massachusetts General Hospital, Harvard Medical School, Boston, Massachusetts. [3]Tokyo Medical and Dental University, Tokyo, Japan. [4]Dana-Farber Cancer Institute, Boston, Massachusetts. [5]Mirati Therapeutics, Inc., San Diego, California.

J.K. Sabari, V. Velcheti, K. Shimizu, and M.R. Strickland contributed as co-first authors and S.C. Kurz, P.K. Brastianos, and H. Wakimoto as co-last authors of this article.

Corresponding Author: Joshua K. Sabari, Laura and Isaac Perlmutter Cancer Center, NYU Langone, New York, NY 10016. Phone: 212-731-5662; E-mail: joshua.sabari@nyulangone.org

Clin Cancer Res 2022;28:3318–28

doi: 10.1158/1078-0432.CCR-22-0383

Translational Relevance

Patients with KRAS-mutant non–small cell lung cancer with brain metastases have a poor prognosis. Here, we report data supporting central nervous system penetration and antitumor activity of adagrasib in preclinical models and in patients harboring brain metastases. These data form the rationale for further clinical development of adagrasib in this patient population. Patients with active, untreated brain metastases are currently being enrolled in a phase Ib cohort of the KRYSTAL-1 trial (NCT03785249).

Adagrasib (MRTX849) is a potent (IC_{50}: 5 nmol/L) covalent inhibitor of $KRAS^{G12C}$ that irreversibly and selectively binds and locks it in its inactive, GDP-bound state (23). Adagrasib was optimized for desirable properties of a $KRAS^{G12C}$ inhibitor, including favorable pharmacokinetic properties, such as oral bioavailability, long half-life (∼24 hours), dose-dependent pharmacokinetics, and extensive tissue distribution (23).

Here, we show the high incidence of BM in patients with KRAS-mutant NSCLC, and present the first data for a $KRAS^{G12C}$ inhibitor supporting CNS penetration and activity in untreated BM, forming the rationale for further clinical development of adagrasib in patients with $KRAS^{G12C}$-mutant NSCLC complicated by BM. We present preclinical evidence of CNS penetration and antitumor activity of adagrasib in murine models of BM. In addition, CSF measurements and preliminary clinical activity of adagrasib in patients with active and untreated BM from a phase Ib cohort of the KRYSTAL-1 trial (NCT03785249) are described.

Materials and Methods

Retrospective analysis of KRAS-mutant NSCLC cohort

This study was performed under an Institutional Review Board–approved protocol (Partners Human Research Protocol #2019P000198). It is standard clinical practice at Massachusetts General Hospital (MGH) to perform comprehensive tumor molecular profiling for all newly diagnosed patients with advanced NSCLC. A retrospective database query of the MGH laboratory information management system identified all patients with NSCLC with KRAS mutations, including the $KRAS^{G12C}$ alteration, treated between May 2015 and October 2019. Inclusion in this retrospective study cohort required an established diagnosis of lung cancer, confirmation of KRAS-mutant disease from any tissue site via molecular profiling, and baseline or serial CNS imaging to determine presence of BM. Electronic medical records were retrospectively reviewed to extract clinicopathologic data, including age, sex, race/ethnicity, smoking history, tumor histologic findings, and disease stage identified at initial presentation, in accordance with the 7th edition of the American Joint Committee on Cancer's Cancer Staging Manual. Programmed death-ligand 1 (PD-L1) was assessed using local testing as per clinical protocol at MGH or confirmed from outside records for patient's referral to MGH after initial work up had already been completed. The distribution of overall survival was summarized using the method of Kaplan–Meier and compared between groups defined by G12C alteration using a log-rank test. The cumulative incidence of BM was estimated in the presence of the competing risk of death without prior BM (24).

Preclinical studies

Cell lines

LU99 and LU65 NSCLC cell lines were obtained from the RIKEN Cell Bank, and the H23 cell line was purchased from the ATCC. Cells were transduced with a lentivirus vector carrying cDNA coding for firefly luciferase to generate LU99-Luc, LU65-Luc, and H23-Luc. All cells were authenticated by short tandem repeat fingerprinting in 2021, and periodically tested to be *Mycoplasma* free.

Animal studies and biosample analysis

Adagrasib, formulated in 10% SBE-b-CD in 50 mmol/L citrate buffer pH 5.0, was dosed orally to 7–9 weeks old female CD-1 mice (WTLH Laboratory Animal Co. Ltd. or SIPPR-B&K Laboratory Animal Co. Ltd.) or 6–7 weeks old female nu/nu mice (Envigo, Livermore) in 10 mg/mL volume. Terminal tissue and blood harvest was performed at 1 and 8 hours after single dose of adagrasib, using 3 mice per timepoint. Sampling procedures and cell permeability assays are described in more detail in the Supplementary Materials and Methods. In brief, whole blood was collected into K2-EDTA tubes and subjected to centrifugation to separate plasma. Brains were collected, rinsed, and homogenized. CSF was collected via needle insertion into the cisterna magna through the occipital membrane, avoiding whole blood contamination. Samples were analyzed using LC/MS-MS using a Triple Quad 6500+ system (AB Sciex LLC). Plasma and tissue concentration versus time data were analyzed by noncompartmental approaches using the Phoenix software program (version 6.3, Pharsight), following method development.

In vivo animal efficacy and pharmacokinetic studies

Murine studies were conducted at the Invicro Molecular Imaging Center (San Diego, CA) or MGH (Boston, MA), and were performed in compliance with all applicable regulations and guidelines of the Institutional Animal Care and Use Committee (IACUC) from the NIH (Bethesda, MD). Mice were maintained under pathogen-free conditions, and food and water were provided *ad libitum*. Six to 7 weeks old female nu/nu mice (Envigo) were implanted intracranially with 1×10^6 LU99-Luc cells in 10 μL serum-free media. The needle was lowered 3 mm into the striatum and left in position for 10–15 seconds before being withdrawn to a 2 mm depth to create a small pocket. The cell suspension was slowly injected by hand with the needle being left in place for 45–60 seconds before complete withdrawal. Mouse health was monitored daily. Fourteen days after implantation, oral twice-daily dosing of 10% captisol in 50 mmol/L citrate buffer pH 5.0 (vehicle) or adagrasib at 100, 30, and 3 mg/kg began and continued for 21 days or until animals required humane euthanasia due to excessive body weight loss or other observations by laboratory personnel as outlined by IACUC guidelines. H23-Luc or LU65-Luc cells (1×10^5 in 2 μL serum-free media) were implanted intracranially (right striatum region) into 6–7 weeks old female nu/nu mice (Charles River Lab). Seven (H23-Luc) or 5 days (LU65-Luc) after implantation, oral twice daily dosing of vehicle or adagrasib at 100 mg/kg was started and continued for 21 days. Animals were euthanized when neurologic deficits and weight loss became significant. CSF pharmacokinetics in non–tumor-bearing athymic mice following 3 days of oral twice daily dosing were tested via cisterna magna puncture, as reported previously (25).

Baseline bioluminescent imaging (BLI) began 24 hours prior to initial dosing with vehicle or adagrasib, and additional imaging timepoints for all animals took place between 18–34 days after inoculation. Animals were injected intraperitoneally with luciferin

(150 mg/kg, 0.01 mL/g) based on body weight and anesthetized using 1%–2% isoflurane in oxygen at 1–2 L/minute. Images were acquired beginning at 10 minutes after luciferin injection. For the pharmacokinetic/pharmacodynamic portion of the study, naïve mice ($n = 3$ per adagrasib dosing level) were used for pharmacokinetic testing. Oral twice daily dosing for 3 days was undertaken, with collection of brain and plasma at 1 hour after last dose or of CSF at 1 and/or 6 hours after dose. In animals with orthotopic intracranial tumors, oral twice daily dosing of vehicle or adagrasib at 100, 30, or 3 occurred for 3 days followed by collection of plasma, tumor, and brain tissue for bioanalytical analysis. For the efficacy portion of the study, $n = 5$ mice (LU99-Luc) or $n = 10$ (LU65-Luc and H23-Luc) per group were enrolled.

Data analysis of efficacy studies in BM animal models

For imaging analysis, region of interest (ROI) analysis was completed on BLI images using VivoQuant software (Invicro). BLI images were generated by overlaying BLI signals for each animal onto their respective white-light images for anatomic reference. Brain ROIs were generated using a fixed-area circle, and were placed on the basis of the BLI signal in the relevant area, using the photographic anatomical reference images. BLI signals in images were scaled in units of radiance (photons per second per square millimeter per steradian). Python software (Python Software Foundation) was used to generate relevant plots based on the VivoQuant quantification. Survival data were collected for each group and analyzed using Kaplan–Meier methodology. Survival duration by group was tested for statistical significance using the log-rank test with FDR correction. Differences in BLI flux on study days 21, 25, and 34 were tested for statistical significance using the Wilcoxon rank-sum test with FDR correction. Statistical comparisons between two groups were considered significant when the adjusted P value was below 0.05.

IHC

Animals harboring H23-Luc or LU65-Luc intracranial tumors were treated with adagrasib (100 mg/kg twice daily) or vehicle for 2 days (four doses) and euthanized 3 hours after the last dosing for brain harvest. Formalin-fixed, paraffin-embedded, 7-μm tissue sections were subjected to microwaving for 15 minutes in 10 mmol/L sodium citrate buffer (pH 6.0) for antigen retrieval, and ImmPRESS polymer detection kits (Vector Laboratories, Inc.) were used for IHC as described previously (26). Slides were incubated overnight at 4°C with the primary antibodies [anti-Ki67 (Agilent Technologies, Inc.) and anti-phospho-ERK (Cell Signaling Technology)]. Ki-67 positivity was determined by counting nuclear positive and negative cells (>200 total cells/slide). Phospho-ERK (pERK) positivity was quantified by using the color deconvolution function in Image J (NIH).

See Supplementary Materials and Methods for pERK modulation determination methods.

KRYSTAL-1 clinical trial

Design and conduct

KRYSTAL-1 is a phase I/II open-label, multicenter study of adagrasib in patients with unresectable or metastatic solid tumors harboring a $KRAS^{G12C}$ mutation that includes multiple dose-escalation and dose-expansion cohorts for treatment with adagrasib as a monotherapy or in combination with other therapies. Patients with $KRAS^{G12C}$-positive NSCLC were treated with the recommended phase II dose of adagrasib orally (600 mg twice daily) administered in a 21-day, continuous dosing regimen until disease progression, unacceptable adverse events, patient refusal, or death. During the phase Ib dose-expansion phase, an expansion cohort of up to 25 patients with $KRAS^{G12C}$-mutant unresectable or metastatic solid tumors with active and untreated BM was implemented. To further evaluate efficacy, patients underwent serial MRI of the brain and, following informed consent, also underwent blood and CSF collection by lumbar puncture at least 6 days after initiating adagrasib. CSF samples were collected 4–6 hours after adagrasib dosing and were immediately frozen at −70°C. Samples were thawed and treated with CHAPS detergent to minimize non-specific binding, and then the concentration was determined using a validated LC/MS-MS method.

Eligibility criteria

The phase Ib limited BM expansion cohort initially included up to 12 patients with neurologically stable, asymptomatic, untreated brain lesions (<2 cm) who were corticosteroid-naïve for ≥2 weeks and not receiving antiepileptic therapy. Although patients with cerebellar metastases and focal leptomeningeal disease were excluded at the start of the trial, the eligibility criteria were expanded to allow enrollment of up to 25 patients with active, untreated BM in the cerebellum and focal leptomeningeal disease. In addition, size restrictions on brain lesions were also removed. Patients with brainstem (midbrain, pons, and medulla) metastases and leptomeningeal carcinomatosis were not eligible for enrollment. Additional eligibility criteria are provided in the Supplementary Materials and Methods.

Trial oversight

The study was approved by an Institutional Review Board or independent ethics committee at each participating site. The trial was conducted in accordance with Good Clinical Practice guidelines, defined by the International Conference on Harmonization. Before the initiation of study procedures, all patients provided written informed consent to participate based on the principles of the Declaration of Helsinki.

Endpoints and assessments

The primary objective of this interim analysis was a preliminary assessment of the CNS accumulation of adagrasib in a subset of patients with active and untreated BM treated with adagrasib 600 mg twice daily orally. Baseline disease assessments were performed at screening using CT or MRI, with a 28-day allowable window. Subsequent on-study disease assessments were performed every 6 weeks from the first dose; these assessments included imaging of all known and suspected disease sites. The imaging modality used (either CT scan or MRI with contrast) was the modality which best evaluated the disease, and the choice was determined by the investigator in conjunction with the local radiologist.

Data availability

Mirati will honor legitimate requests for clinical trial data from qualified researchers, upon request, as necessary for conducting methodologically sound research. Mirati will provide access to data and clinical study reports for clinical trials for which results are posted on the clinicaltrials.gov registry for products or indications that have been approved by regulators in the United States and European Union. In general, data will be made available for request approximately 12 months after clinical trial completion.

Results

Patients with KRAS-mutant NSCLC have a high propensity to develop BM

To better understand the clinicopathologic features of patients with KRAS-mutant NSCLC as they pertain to BM, we performed a

retrospective database analysis on patients with KRAS-mutant lung cancer treated at MGH between May 2015 and October 2019 (Supplementary Table S1) and for whom tumor tissue molecular profiling was completed. A total of 374 patients were analyzed; 40% ($n = 149$) harbored $KRAS^{G12C}$ mutations while 60% ($n = 225$) had KRAS-mutant non-G12C disease. Average age at initial lung cancer diagnosis was 68 years (range, 29–91). The majority of patients were female (58%), White (88%), and heavy smokers (defined as >10 pack-years; 82%). Eighty-five percent ($n = 318$) of patients had a histologic diagnosis of adenocarcinoma and 67% ($n = 249$) had stage IV disease at the time of initial cancer diagnosis. There were no statistically significant differences in age, sex, ethnicity, smoking history and/or tumor histology between G12C and non-G12C patients. Overall, 40% ($n = 150$) of patients developed BM at any time and there was no difference in BM frequency by genotype [40% ($n = 60$) for G12C and 40% ($n = 90$) for non-G12C patients, $P = 0.97$]. A greater proportion of patients harboring G12C disease had an Eastern Cooperative Oncology Group performance status of 0 or 1 (71%, $n = 105$) versus patients with non-G12C disease (63%, $n = 141$), which met statistical significance ($P = 0.04$).

Cumulative incidence of BM in patients with KRAS-mutant (G12C vs. non-G12C) disease was determined using a model with death without prior BM as competing risk. In the subgroup of patients that developed metastatic disease at any time ($n = 287$), 6-month cumulative incidence of BM since time of initial diagnosis of metastatic disease was 42.2% [95% confidence interval (CI), 33–51] and 41.9% (95% CI, 34–49) for G12C and non-G12C status, respectively; 12-month cumulative incidence was 48.2% (95% CI, 38–57) and 46.6% (95% CI, 38–54) for G12C and non-G12C status, respectively (**Fig. 1A**). Most patients (77%, $N = 116$) demonstrated synchronous BM diagnoses defined as detection within 3 months of initial diagnosis of metastatic disease while 23% ($n = 34$) developed metachronous BM. Cumulative incidence of metachronous BM for patients with $KRAS^{G12C}$ disease (death without prior BM or synchronous BM were used as competing risks) was 6.1% (95% CI, 2–13) at 12 months and 7.4% (95% CI, 3–15) at 24 months (**Fig. 1B**). Median overall

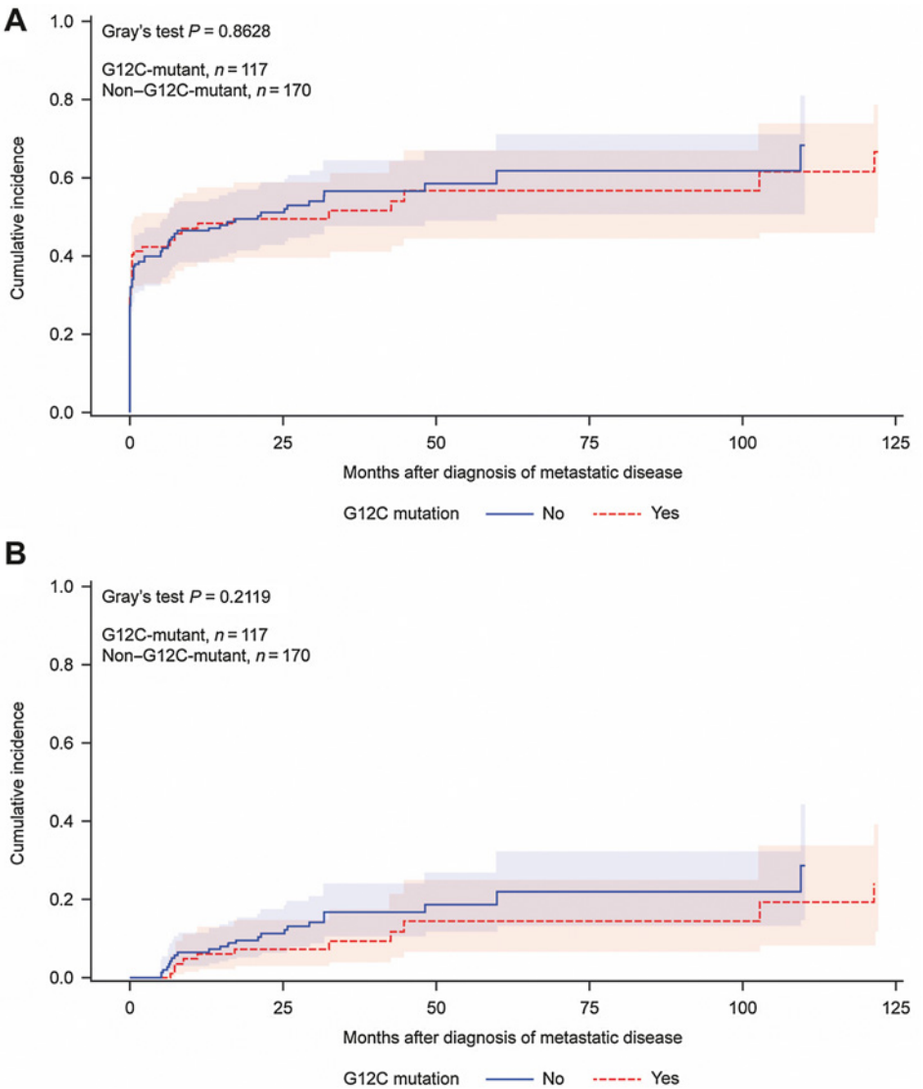

Figure 1.

A, Cumulative incidence of brain metastasis since time of initial diagnosis of metastatic disease in patients with KRAS-mutant lung cancer ($n = 287$); a competing risk model was used with death without prior brain metastasis as competing risk. **B,** Cumulative incidence of metachronous brain metastasis in patients with KRAS-mutant lung cancer since time of initial diagnosis of metastatic disease ($n = 34$); a model with death without prior brain metastasis and synchronous BM as competing risks was used.

survival among patients with $KRAS^{G12C}$ lung cancer since time of initial diagnosis of metastatic disease (Supplementary Fig. S1) was 19.1 months (95% CI, 12–29) which did not differ significantly compared with patients with KRAS non–G12C-mutant disease (18.8 months; 95% CI, 13–26; $P = 0.85$). Collectively, these data indicate the high propensity of patients with KRAS-mutant NSCLC—particularly those with G12C alterations—to develop BM. The majority of BM were found synchronously at initial diagnosis of metastatic disease in these patients.

Preclinical studies

Properties of adagrasib enable CNS penetration

As particular physiochemical and absorption, distribution, metabolism, and excretion (ADME) properties are known to influence CNS penetration of small molecules, we evaluated these properties of adagrasib *in vitro* and in a mouse model. P-glycoprotein (P-gp, MDR), an efflux transporter that actively transports lipophilic drugs out of the CSF, is an important gatekeeper of CNS penetration (27). Thus, we measured adagrasib concentration-dependent efflux ratio and P-gp inhibition in MDCK-MDR cell permeability assays. The efflux ratio was determined to be 13, which ostensibly, suggests limited CNS exposure. However, the IC_{50} for P-gp inhibition was 980 nmol/L indicating that adagrasib demonstrated concentration-dependent inhibition of its own efflux within a physiologically relevant range. This inhibition is anticipated to bypass physicochemical/ADME constraints of the blood-brain barrier allowing adagrasib to gain access to the CNS (**Table 1**).

Adagrasib at clinically achievable concentrations penetrates mouse CNS

To measure whether adagrasib could penetrate the CNS at a clinically relevant dose level, mice were treated with a single oral dose of 100 or 200 mg/kg adagrasib. Adagrasib total and free-plasma concentrations were 8.6 μmol/L and 43 nmol/L, respectively, at 8 hours following a 200 mg/kg dose; in mice, this dose yields sustained free-fraction adjusted plasma exposure comparable with mean steady-state clinical human free-plasma concentrations (43.6 nmol/L) at 600 mg twice daily (the phase II dose of adagrasib; **Table 1**). In addition, CSF levels in mice were above the IC_{50} for at least 8 hours after dose and levels of adagrasib in CSF (52 nmol/L) were comparable with free fraction–adjusted levels observed in plasma at the 200 mg/kg dose (**Table 1**). At the 200 mg/kg dose level in mice, the unbound brain to unbound plasma concentration ratio ($K_{p,uu}$) value was approximately 1 at 8 hours indicating significant penetration into CNS at this dose level. To evaluate dose-dependent CNS exposure in a concentration range approaching levels achieved in humans, and to support repeat-administration studies in mouse models, a 100 mg/kg dose level of adagrasib was also evaluated. At 1 and 8 hours after adagrasib administration at 100 mg/kg, the mean plasma concentrations (free-fraction adjusted) were 46.8 and 43.3 nmol/L, respectively, which are also comparable with clinical steady-state human average free-plasma concentrations at 600 mg twice daily (**Fig. 2A**; **Table 1**; ref. 28). Also at the 100 mg/kg dose level, the mean CSF concentrations at 1 and 8 hours after dose were 19.1 nmol/L ($K_{p,uu}$ 0.4) and 7.4 nmol/L ($K_{p,uu} \sim 0.2$), respectively, each of which exceeded the cellular IC_{50} of adagrasib (**Fig. 2A**; **Table 1**; ref. 29). CSF concentrations of adagrasib were measured in an additional mouse model following 3 days of treatment at 100 mg/kg twice daily (Supplementary Fig. S2A). The observation that the $K_{p,uu}$ value was approximately 1 at the 200 mg/kg dose level and 0.2–0.4 at the 100 mg/kg level indicate that both time- and dose-dependent penetration into CNS was observed in mice, and that levels achieved at the 200 mg/kg dose level result in near complete saturation of P-gp–dependent efflux, thereby maximizing CNS exposure. Overall, these data suggest that the observed exposures with adagrasib are sufficient to achieve CNS penetration at clinically achievable concentrations *in vivo*.

Table 1. Selected physiochemical and ADME properties of adagrasib (23, 28, 29).

Parameter	Value
Cellular mechanistic assay (pERK) IC_{50}, nmol/L	5
Plasma protein binding (human), %	99
Molecular weight, g/mol	604
MDCK-MDR efflux ratio (2 μmol/L)	13
MDCK-MDR P-gp inhibition (IC_{50}), nmol/L	980
Total plasma concentration at 8 hours (200 mg/kg orally; mouse)[a], nmol/L	8,600
Free plasma concentration at 8 hours (200 mg/kg orally; mouse)[b], nmol/L	43
CSF concentration at 8 hours (200 mg/kg orally; mouse)[b], nmol/L	52
Total C_{ave} at steady state at 600 mg twice daily (human), nmol/L (ng/mL)	4,362 (2,635)
Free-fraction adjusted C_{ave} (human), nmol/L	43.6

Abbreviations: ADME, absorption, distribution, metabolism, excretion; C_{ave}, average plasma concentration; CSF, cerebrospinal fluid; nmol/L, nanomolar; P-gp, P-glycoprotein.

[a]Mouse CNS exposure at 8 hours is similar to the human average free plasma concentration at 600 mg twice daily.

[b]A total of 200 mg/kg dose of adagrasib results in CSF exposure above the IC_{50} for >8 hours; plasma protein binding (mouse), 99.5%.

Adagrasib achieves tumor regression in BM models

To determine whether adagrasib brain and CSF exposure was sufficient to mediate regression of tumors in experimental BM models, we treated mice bearing intracranially implanted LU99-Luc $KRAS^{G12C}$-mutant tumors with adagrasib 100 mg/kg twice daily; this was intended to reflect human steady-state average observed plasma concentrations and normalize peak-to-trough variation in mice to be more consistent with human plasma exposure profiles (**Fig. 2B**). Adagrasib exhibited dose-dependent pharmacokinetic and reduction of phosphorylated ERK1/2 (**Fig. 2C**), and this translated into near complete tumor regression in the brain as evidenced by BLI at the 100 mg/kg twice daily (200 mg/kg/day) dose level (**Fig. 2C** and **D**). In addition, adagrasib at 100 mg/kg twice daily demonstrated an increase in overall survival ($P < 0.05$), with 2 of 5 animals having no measurable tumor detected by either BLI or MRI, indicating complete responses (**Fig. 2E**).

Anti-BM activity of adagrasib in additional preclinical models

We next determined the antitumor activity of 100 mg/kg twice daily treatment of adagrasib using additional preclinical models of $KRAS^{G12C}$-mutant NSCLC BM. In mice bearing intracranial xenografts of H23-Luc, oral adagrasib dosing resulted in accumulation in plasma, brain, and tumors (**Fig. 3A**). Using intracranial $KRAS^{G12C}$-mutant NSCLC xenografts of LU65-Luc and H23-Luc, we showed that daily adagrasib 100 mg/kg twice daily treatment for 21 days resulted in significant inhibition of brain tumor growth revealed by BLI (**Fig. 3B–E**; Supplementary Fig. S2B–S2D and S3A–S3E). LU65-Luc xenografts responded particularly well to the treatment, as evidenced by dramatic

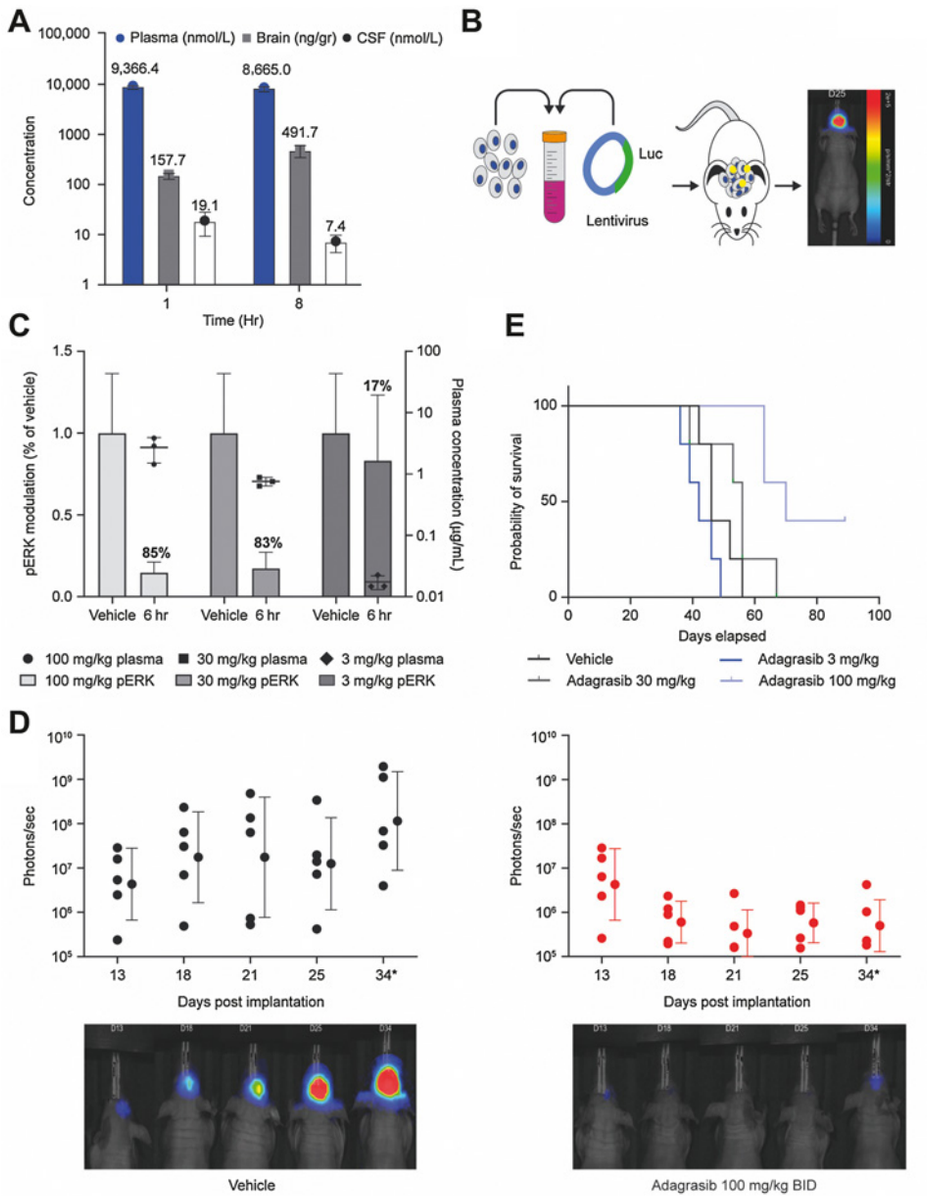

Figure 2.

A, Adagrasib 100 mg/kg was administered orally to CD-1 mice, followed by harvest of blood, brain, and CSF at 1 and 8 hours after dose. Drug levels of adagrasib in the plasma (nmol/L), brain homogenate (ng/gr), and CSF (nmol/L) are shown from $n = 3$ mice as mean ± SD. **B,** A human NSCLC cell line with a known $KRAS^{G12C}$ mutation, LU99, was stably transfected with luciferase to allow for BLI. The LU99-Luc cells were implanted intracranially into mice on day 0, and animals were enrolled into the efficacy study design based on baseline BLI intensities. ROIs were determined on the basis of signal intensity. **C,** Animals bearing LU99-Luc intracranial tumors were enrolled into a pharmacokinetic/pharmacodynamic arm of the study and treated with oral vehicle or adagrasib 100, 30, and 3 mg/kg twice daily (BID) for 3 days, followed by blood, tumor, and brain collection at 6 hours after the final dose. pERK modulation in the tumor and adagrasib plasma concentration data from $n = 3$ mice are shown as mean ± SD. **D,** Enrolled study animals were treated with oral vehicle or adagrasib 100 mg/kg twice daily for 21 days from day 1. BLI occurred on days 13, 18, and 21 while on treatment, and continued on days 25 and 34 after treatment stopped. BLI signal for each subject was determined at day indicated and scaled in units of radiance, defined as photons per second per square millimeter per steradian (p/second/mm^2/str) and plotted with VivoQuant and Python software. Error bars indicate geometric mean ± geometric SD from $n = 5$ mice per group. Individual animal BLI images shown are representative of the group. BLI flux was significant ($P_{adjusted} < 0.05$) on day 34 by Wilcoxon rank-sum test with FDR correction. **E,** Survival data were collected for each group ($n = 5$/group) out to 76 days after implantation and analyzed by Kaplan–Meier statistical analysis. The remaining subjects in the adagrasib 100 mg/kg dose group were euthanized on day 91. A statistically significant increase in survival was observed only in mice dosed with 100 mg/kg adagrasib compared with vehicle using the log-rank test with FDR correction ($P_{adjusted} < 0.05$).

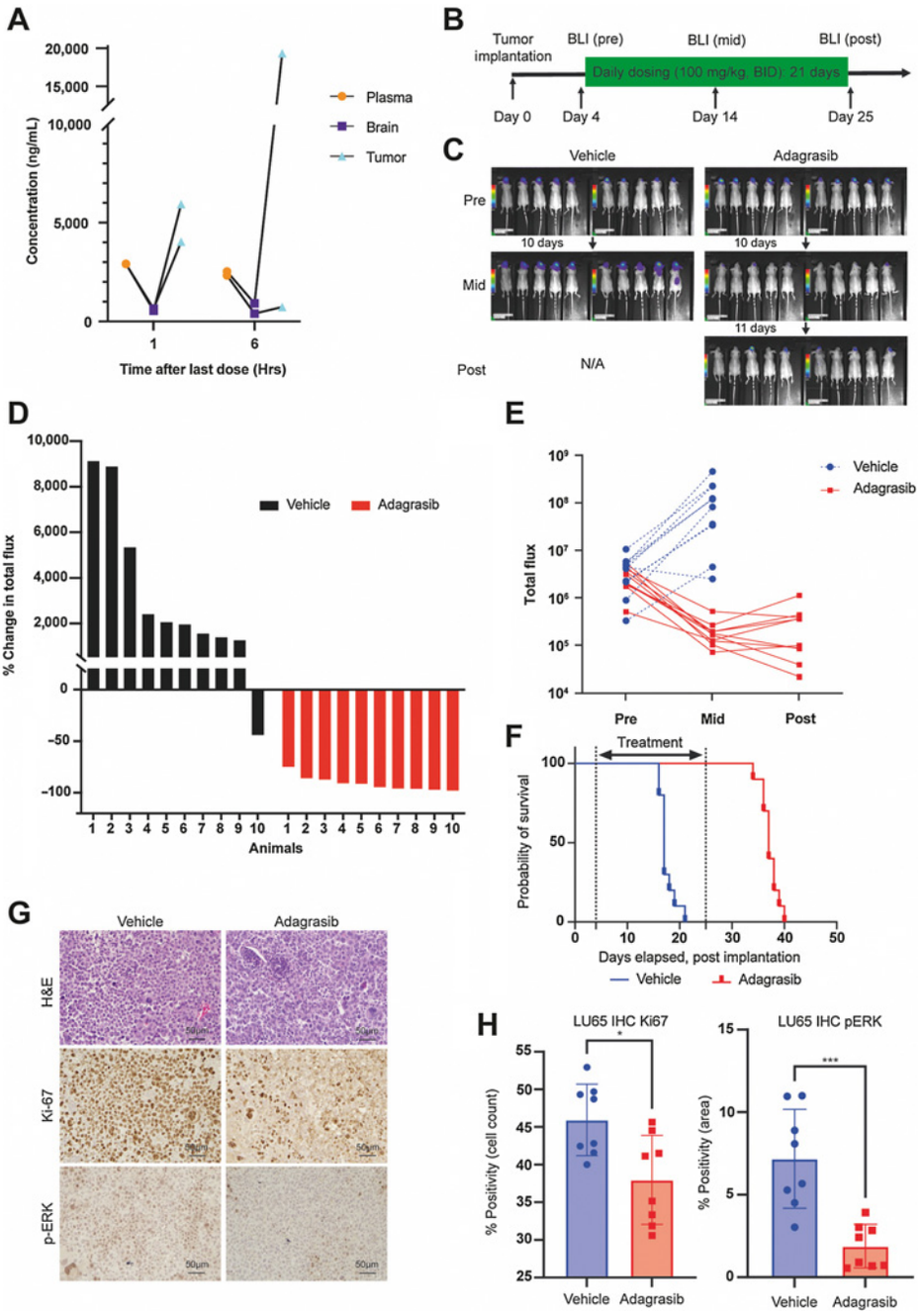

Figure 3.
Characterization of the antitumor effects of adagrasib in H23 and LU65 brain tumor models *in vivo*. **A,** Pharmacokinetics of adagrasib in mice bearing intracranial H23-Luc non–small cell lung adenocarcinoma. Adagrasib was administered for 3 days at 100 mg/kg twice daily; tissues were harvested 1 or 6 hours after last dose. Data from the same animal are connected by lines. **B,** Experimental schematic of drug efficacy study in the intracranial LU65-Luc model ($n = 10$/group) **C,** BLI of LU65-Luc tumors in mice before and after the 3-week-long daily drug treatment. **D,** Waterfall plot analysis of drug effects *in vivo*, indicating percent change in total bioluminescence flux in individual animals in the two groups. **E,** The ratio of pre and post total bioluminescence flux signal, comparing the two groups. Each data point represents a tumor. **F,** Probability of survival after implantation ($P < 0.0001$ by log-rank test). **G,** Representative microscopic images of IHC for Ki-67 and p-ERK in intracranial LU65 tumors after 2-day treatment of mice. **H,** Quantification of percent positivity of Ki-67 and p-ERK IHC. The Mann–Whitney test was used for comparison.

tumor regression (**Fig. 3C–E**; Supplementary Fig. S2B–S2D) and prolongation of animal survival (**Fig. 3F**; median survival time: vehicle, 17 days vs. adagrasib, 37 days, $P < 0.0001$). Survival extension did not reach statistical significance in the H23-Luc model as a fraction of vehicle-treated mice had longer survival (Supplementary Fig. S3F). Adagrasib 100 mg/kg twice daily treatment was well tolerated with minimal sign of overt toxicity or animal weight loss (Supplementary Fig. S2E). In line with these potent anti-BM effects, adagrasib significantly decreased MAPK activation (pERK) and proliferation (Ki-67) in the brain in both $KRAS^{G12C}$-mutant NSCLC models, providing critical on-target pharmacodynamic evidence (**Fig. 3G** and **H**; Supplementary Fig. S3G and S3H). Together, these data demonstrate target pathway inhibition, tumor regression, and increased survival in multiple BM mouse models treated with a clinically relevant dose of adagrasib.

Activity of adagrasib in patients with BM

KRYSTAL-1 phase Ib active and untreated BM cohort

The preliminary analysis of adagrasib CSF accumulation and potential clinical activity reported here focuses on the 2 patients with

metastatic $KRAS^{G12C}$-mutant NSCLC receiving adagrasib 600 mg twice daily, who were enrolled in the phase Ib limited BM cohort of KRYSTAL-1 who had CSF data available. The average $K_{p,uu}$ in these 2 patients was calculated at 0.47.

Case 1

A 67-year-old female (current smoker) was diagnosed with stage IIIA NSCLC (adenocarcinoma) and started treatment with neoadjuvant carboplatin and pemetrexed 1 month later (**Fig. 4**). Three months after diagnosis metastases developed in the lungs, lymph nodes, vertebral body, and brain. The patient then received palliative radiotherapy initiated to the left humerus and T8 vertebral body bone lesions, 2,000 cGy over five fractions. The following month the patient enrolled in the phase Ib cohort of the KRYSTAL-1 trial enrolling patients with active and untreated brain metastases. Following two cycles of adagrasib, the best overall response was a partial response (−31% on systemic measurements) and they experienced the disappearance of three brain lesions (compared with baseline) by imaging. This patient also had a CSF concentration of adagrasib of 34.6 nmol/L [20.9 ng/mL; at steady state and at peak (4–6 hours after dose) following at least 6 days of adagrasib treatment], which was consistent with CSF measurements demonstrated in preclinical models. Treatment-related AEs were nausea, diarrhea, vomiting, increased alanine aminotransferase, increased aspartate aminotransferase, increased creatinine, and dehydration; all of which were grade 1 or 2 in severity.

Case 2

A 66-year-old male with previous smoking history was diagnosed with metastatic NSCLC with BM (**Fig. 5**). In the month following diagnosis, the patient received palliative radiation to his L5 bone lesion, followed by carboplatin, pemetrexed, and pembrolizumab until progressive disease was noted. Four months after diagnosis with metastatic disease, the patient enrolled in the phase Ib cohort of the KRYSTAL-1 trial enrolling patients with active and untreated brain metastases. Following two cycles of adagrasib, the best overall response was stable disease (−16.7% on systemic measurements) and the patient experienced decreases in the size of three brain lesions (compared with baseline) by imaging. This patient also had a CSF concentration of adagrasib of 24.2 nmol/L (14.6 ng/mL; at steady state), which was consistent with CSF measurements demonstrated in preclinical models. Treatment-related AEs were grade 1 or 2 nausea, diarrhea, increased creatinine, and dysgeusia, and a grade 3 acneiform rash.

Discussion

Development of BM is typically associated with poor outcomes for patients with cancer, and represents an area of great unmet need (5–7). Advances in targeted therapies suggest that agents with increased CNS bioavailability, such as lorlatinib, alectinib, and osimertinib, may be more effective in preventing and treating BM in NSCLC (12–15). Therapies specifically targeting the $KRAS^{G12C}$-mutant protein include sotorasib and adagrasib; however, despite their common target, these agents differ in their properties. Adagrasib has been optimized for favorable pharmacokinetic properties, including CNS penetration, and the preliminary data presented here are the first to be published on the effect of a $KRAS^{G12C}$ inhibitor on CNS-specific activity in preclinical models of BM and in patients with untreated BM, supporting further investigation of adagrasib in this setting. The CNS-penetrative capacity of sotorasib and its activity in untreated BM has not yet been fully characterized.

The retrospective analysis of patients with KRAS-mutant lung cancer treated at MGH showcases the high propensity of patients with KRAS-mutant NSCLC to develop BM. While the majority of

Demographics
• 67-year-old female with stage IIIA NSCLC (adenocarcinoma)
• Current smoker
Treatment History
• Treated with neoadjuvant carboplatin + pemetrexed for 2 months after diagnosis
• Three months after diagnosis, the patient developed metastases (lung, lymph node, vertebral body, and brain lesions)
• The patient received palliative radiotherapy initiated to the left humerus and T8 vertebral body bone lesions, 2,000 cGy over 5 fractions
• Four months after diagnosis, the patient enrolled in the Phase 1b cohort of the KRYSTAL-1 trial and started adagrasib 600 mg BID
Best Response
• Following 2 cycles of adagrasib, best overall response was a partial response (–31% based on systemic disease measurements)
• Disappearance of 3 brain lesions (compared with baseline) by imaging
CSF
• 34.6 nmol/L (20.9 ng/mL)
Treatment-related Adverse Events
• Grade 1 or 2 nausea, diarrhea, vomiting, increased alanine aminotransferase, increased aspartate aminotransferase, increased creatinine, and dehydration

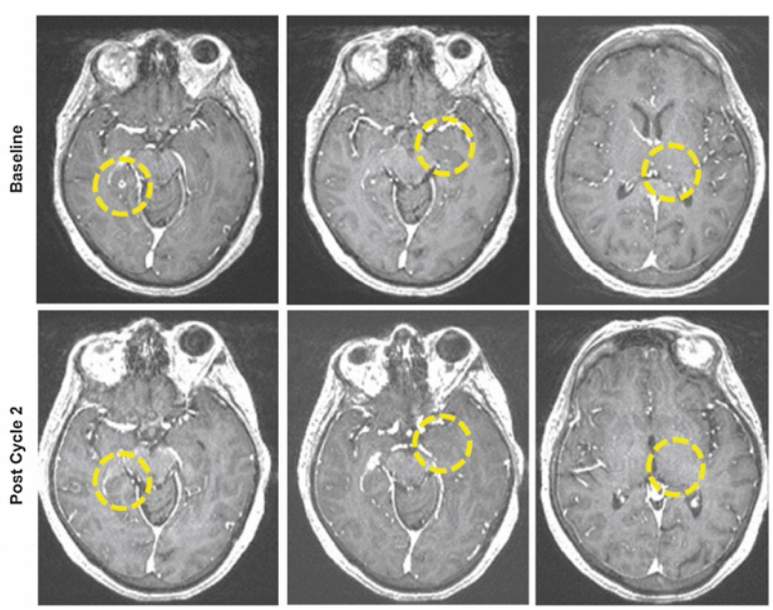

Figure 4.
Case 1.

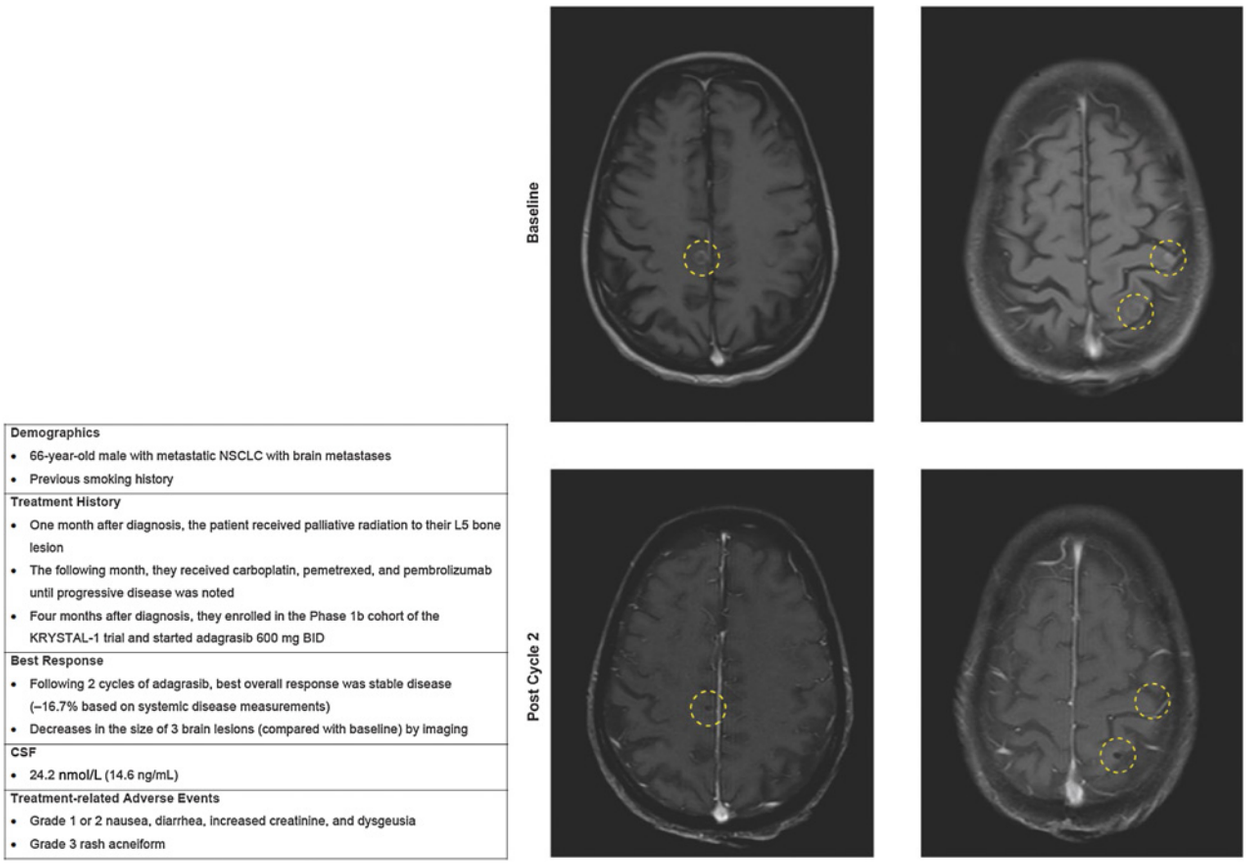

Figure 5.
Case 2.

BM in these patients were found synchronously with respect to the initial diagnosis of metastatic disease, a clinically significant subset of patients developed metachronous BM subsequent to detection of metastatic disease. Of all patients in our cohort with $KRAS^{G12C}$-mutant disease, 40% developed BM at any time, highlighting the high incidence of BM within this patient population. To account for the bias of competing risk of death without prior BM, a competing risk model was utilized to assess cumulative incidence of BM over time and demonstrated consistent trends. Potential limitations of this analysis include its retrospective design and relatively small sample size. Furthermore, the cohort did not include patients with KRAS wildtype NSCLC and thus comparisons can be made only among KRAS-mutant (G12C vs. non-G12C) genotypes. To better understand BM frequencies across different genotypes within NSCLC patient populations, future analyses should explore inclusion of patients with KRAS wildtype tumors. Finally, while all patients had baseline CNS imaging, those without CNS disease detected did not subsequently receive CNS surveillance imaging consistent with standard of care. Thus, development of asymptomatic, metachronous BM may have been undetected resulting in an underestimation of frequency in this cohort. Nonetheless, given the high incidence of BM, this patient population is uniquely poised to derive benefit from a CNS-penetrant, $KRAS^{G12C}$ inhibitor with activity across both intracranial and extracranial compartments.

The preclinical studies presented here support that the properties of adagrasib allow it to bypass the physiochemical constraints of the blood–brain barrier, enabling its penetration into the CNS. Adagrasib access to the CNS is predicted to be at least partially mediated by its inhibition of P-gp–mediated efflux, as it is both a substrate and inhibitor of P-gp at clinically achievable concentrations. The observed adagrasib systemic plasma exposure in nonclinical models was sufficient to achieve CNS penetration at clinically achievable concentrations *in vivo*. Furthermore, adagrasib demonstrated dose-dependent brain and CSF exposure with clinically relevant dose levels in nonclinical models *in vivo*. The CSF concentrations and measured $K_{p,uu}$ values (range, ∼0.2–1) determined in a clinically relevant dose range in mouse models are also reflective of CNS access. Importantly, we demonstrated target pathway inhibition, tumor regression, and increased survival in multiple BM mice models after treatment with a clinically relevant oral dose of adagrasib. Different coexisting genetic alterations (e.g., CDKN2A homozygous deletion in LU99, and STK11 mutation in H23 and LU65) present in the preclinical xenograft models used herein support a broad applicability of adagrasib to $KRAS^{G12C}$-mutant NSCLC with BM (23, 30). As the intracranial implantation models do not recapitulate the pathophysiologic process of blood-borne establishment of metastatic lesions in the CNS, additional work is ongoing in models induced by intracardiac injection of cancer cells (31). In addition, rational combination strategies in

different genetic contexts guided by comutation of additional actionable genetic cancer drivers (such as CDKN2A deletion) will require exploration, to enhance efficacy and mitigate emergence of acquired resistance mechanisms (32, 33).

Preliminary clinical data from 2 patients enrolled in the KRYSTAL-1 untreated BM cohort demonstrated that concentrations of adagrasib in CSF were above the target cellular IC_{50}. In addition, the mean $K_{p,uu}$ value determined for these patients (0.47) was consistent with observations of exposure and antitumor activity in nonclinical models and also exceeds values for the TKIs for which both CNS penetration and antitumor activity in BM have previously been demonstrated (16–18). Furthermore, BM regression was observed in both patients. The treatment-related AEs reported in these patients were mostly grade 1 or 2 in severity and no new safety signals were observed. While preliminary, and in a very small number of patients, these data support further clinical development of adagrasib in patients with $KRAS^{G12C}$-mutant NSCLC with active and untreated BM.

In summary, our data suggest that patients with $KRAS^{G12C}$-mutant NSCLC have a high incidence of developing BM. Multiple *in vivo* models and early clinical data suggest adagrasib penetrates the CNS; moreover, in 2 patients with NSCLC with active and untreated BM, adagrasib led to the regression of lesions compared with baseline. Further evaluations are ongoing to assess the clinical activity of adagrasib in this patient population as well as to elucidate intracranial response via standardized CNS imaging criteria, durability, and outcomes in larger numbers of patients (KRYSTAL-1 trial, NCT03785249). Overall, these data provide the first proof-of-concept preclinical and clinical data for a CNS-penetrant $KRAS^{G12C}$ inhibitor and support additional clinical development in this patient population.

Authors' Disclosures

J.K. Sabari reports personal fees from AstraZeneca, Genentech Roche, Janssen, Navire, Pfizer, Regeneron, and Sanofi Genzyme and personal fees and other support from Takeda outside the submitted work. V. Velcheti reports personal fees from BMS, Merck, AstraZeneca, Amgen, and Foundation Medicine outside the submitted work. R.S. Heist reports other support from AbbVie, EMD Serono, Daichii Sankyo, and Novartis and grants from AbbVie, Novartis, Daichii Sankyo, Turning Point, Agios, Mirati, Corvus, Genentech Roche, Exelixis, and Lilly outside the submitted work. S.R. Digumarthy reports grants from Lunit Inc, GE, Qure AI, and Vuno and other support from Siemens outside the submitted work; in addition, S.R. Digumarthy provides independent image analysis for hospital-contracted clinical research trials and programs for Merck, Pfizer, Bristol Myers Squibb, Novartis, Roche, Polaris, Cascadian, AbbVie, Gradalis, Bayer, Zai Laboratories, Biogen, Resonance, and Analise. J.F. Gainor reports personal fees and other support from Bristol-Myers Squibb, Merck, Genentech/Roche, AstraZeneca, Moderna, and Blueprint and personal fees from Loxo/Lilly, Mirati, Pfizer, EMD Serono, iTeos, Novartis, Karyopharm, Beigene, Nuvalent, GlydeBio, and Silverback Therapeutics outside the submitted work; in addition, J.F. Gainor has an immediate family member who is an employee with equity in Ironwood Pharmaceuticals. A.C. Burns reports personal fees from Mirati Therapeutics outside the submitted work. P. Olson reports other support from Mirati Therapeutics during the conduct of the study. J.G. Christensen reports personal fees from Mirati Therapeutics during the conduct of the study as well as personal fees from Mirati Therapeutics outside the submitted work; in addition, J.G. Christensen has U.S. Patent No. 10,689,377 issued to Mirati Therapeutics. P.K. Brastianos reports grants from Mirati, Breast Cancer Research Foundation, NIH, Damon Runyon Cancer Research Foundation, Ben and Catherine Ivy Foundation, Demetra Fund of the Hellenic Women's Association, and Terry and Jean de Gunzburg MGH Research Scholar Award during the conduct of the study as well as personal fees from Advise Connect Inspire, Dantari, Elevatebio, Pfizer, SK Life Sciences, Voyager Therapeutics, and Sintetica and grants and non-financial support from Merck, Lilly, BMS, Pfizer, AstraZeneca, Kazia, Genentech-Roche, and GSK outside the submitted work. H. Wakimoto reports other support from Mirati Therapeutics during the conduct of the study. No disclosures were reported by the other authors.

Authors' Contributions

J.K. Sabari: Resources, data curation, formal analysis, supervision, validation, investigation, writing–original draft, writing–review and editing. **V. Velcheti:** Resources, data curation, formal analysis, validation, investigation, writing–original draft, writing–review and editing. **K. Shimizu:** Resources, data curation, formal analysis, validation, investigation, writing–original draft, writing–review and editing. **M.R. Strickland:** Resources, data curation, formal analysis, validation, investigation, writing–original draft, writing–review and editing. **R.S. Heist:** Resources, data curation, formal analysis, supervision, validation, investigation, writing–original draft, writing–review and editing. **M. Singh:** Resources, data curation, investigation, writing–original draft, writing–review and editing. **N. Nayyar:** Resources, data curation, formal analysis, validation, investigation, writing–original draft, writing–review and editing. **A. Giobbie-Hurder:** Resources, data curation, formal analysis, validation, investigation, writing–original draft, writing–review and editing. **S.R. Digumarthy:** Resources, data curation, supervision, writing–original draft, writing–review and editing. **J.F. Gainor:** Resources, data curation, supervision, investigation, writing–original draft, writing–review and editing. **A.P. Rajan:** Data curation, formal analysis, validation, investigation, writing–original draft, writing–review and editing. **E. Nieblas-Bedolla:** Data curation, formal analysis, validation, investigation, writing–original draft, writing–review and editing. **A.C. Burns:** Resources, data curation, formal analysis, validation, investigation, writing–original draft, writing–review and editing. **J. Hallin:** Resources, data curation, formal analysis, validation, investigation, writing–original draft, writing–review and editing. **P. Olson:** Formal analysis, validation, investigation, methodology, writing–original draft, writing–review and editing. **J.G. Christensen:** Conceptualization, formal analysis, supervision, validation, investigation, methodology, writing–original draft, writing–review and editing. **S.C. Kurz:** Resources, data curation, formal analysis, validation, investigation, writing–original draft, writing–review and editing. **P.K. Brastianos:** Conceptualization, resources, data curation, formal analysis, supervision, funding acquisition, validation, investigation, methodology, writing–original draft, writing–review and editing. **H. Wakimoto:** Conceptualization, formal analysis, supervision, funding acquisition, validation, investigation, methodology, writing–original draft, writing–review and editing.

Acknowledgments

This project was funded by Mirati Therapeutics, Inc. and P.K. Brastianos through financial support from the NIH (5R01CA227156-02), Damon Runyon Cancer Research Foundation, the Ben and Catherine Ivy Foundation, Breast Cancer Research Foundation, Demetra Fund of the Hellenic Women's Association, and the Terry and Jean de Gunzburg MGH Research Scholar Award. The authors would like to thank Lauren Hargis for her excellent technical assistance. Invicro provided technical assistance funded by Mirati Therapeutics, Inc. The authors would also like to thank Aaditya Gupta for his work and Gregory Wojtkiewicz for animal imaging at Massachusetts General Hospital. Medical writing and editorial support were provided by Alex Coulthard of Ashfield MedComms, an Ashfield Health company, and was funded by Mirati Therapeutics, Inc.

The publication costs of this article were defrayed in part by the payment of publication fees. Therefore, and solely to indicate this fact, this article is hereby marked "advertisement" in accordance with 18 USC section 1734.

Note

Supplementary data for this article are available at Clinical Cancer Research Online (http://clincancerres.aacrjournals.org/).

Received February 3, 2022; revised March 7, 2022; accepted April 4, 2022; published first April 11, 2022.

References

1. Simanshu DK, Nissley DV, McCormick F. RAS proteins and their regulators in human disease. Cell 2017;170:17–33.
2. Cancer Genome Atlas Research Network. Comprehensive molecular profiling of lung adenocarcinoma. Nature 2014;511:543–50.

3. Zehir A, Benayed R, Shah RH, Syed A, Middha S, Kim HR, et al. Mutational landscape of metastatic cancer revealed from prospective clinical sequencing of 10,000 patients. Nat Med 2017;23:703–13.
4. Dinu D, Dobre M, Panaitescu E, Birla R, Iosif C, Hoara P, et al. Prognostic significance of KRAS gene mutations in colorectal cancer–preliminary study. J Med Life 2014;7:581–7.
5. Offin M, Feldman D, Ni A, Myers ML, Lai WV, Pentsova E, et al. Frequency and outcomes of brain metastases in patients with HER2-mutant lung cancers. Cancer 2019;125:4380–7.
6. Liu Q, Tong X, Wang J. Management of brain metastases: history and the present. Chin Neurosurg J 2019;5:1.
7. Mehta MP, Rodrigus P, Terhaard CH, Rao A, Suh J, Roa W, et al. Survival and neurologic outcomes in a randomized trial of motexafin gadolinium and whole-brain radiation therapy in brain metastases. J Clin Oncol 2003;21:2529–36.
8. Cui W, Franchini F, Alexander M, Officer A, Wong HL, IJ M, et al. Real world outcomes in KRAS G12C mutation positive non-small cell lung cancer. Lung Cancer 2020;146:310–7.
9. Wu MY, Zhang EW, Strickland MR, Mendoza DP, Lipkin L, Lennerz JK, et al. Clinical and imaging features of non-small cell lung cancer with G12C KRAS mutation. Cancers 2021;13:3572.
10. Sebastian M, Eberhardt WEE, Hoffknecht P, Metzenmacher M, Wehler T, Kokowski K, et al. KRAS G12C-mutated advanced non-small cell lung cancer: a real-world cohort from the German prospective, observational, nation-wide CRISP Registry (AIO-TRK-0315). Lung Cancer 2021;154:51–61.
11. Lee JS, Hong JH, Sun S, Won HS, Kim YH, Ahn MS, et al. The impact of systemic treatment on brain metastasis in patients with non-small-cell lung cancer: a retrospective nationwide population-based cohort study. Sci Rep 2019;9:18689.
12. Peters S, Camidge DR, Shaw AT, Gadgeel S, Ahn JS, Kim DW, et al. Alectinib versus crizotinib in untreated ALK-positive non-small-cell lung cancer. N Engl J Med 2017;377:829–38.
13. Bauer TM, Shaw AT, Johnson ML, Navarro A, Gainor JF, Thurm H, et al. Brain penetration of lorlatinib: cumulative incidences of CNS and non-CNS progression with lorlatinib in patients with previously treated ALK-positive non-small-cell lung cancer. Target Oncol 2020;15:55–65.
14. Goss G, Tsai CM, Shepherd FA, Ahn MJ, Bazhenova L, Crino L, et al. CNS response to osimertinib in patients with T790M-positive advanced NSCLC: pooled data from two phase II trials. Ann Oncol 2018;29:687–93.
15. Soffietti R, Ahluwalia M, Lin N, Ruda R. Management of brain metastases according to molecular subtypes. Nat Rev Neurol 2020;16:557–74.
16. Ballard P, Yates JW, Yang Z, Kim DW, Yang JC, Cantarini M, et al. Preclinical comparison of osimertinib with other EGFR-TKIs in EGFR-mutant NSCLC brain metastases models, and early evidence of clinical brain metastases activity. Clin Cancer Res 2016;22:5130–40.
17. Kodama T, Hasegawa M, Takanashi K, Sakurai Y, Kondoh O, Sakamoto H. Antitumor activity of the selective ALK inhibitor alectinib in models of intracranial metastases. Cancer Chemother Pharmacol 2014;74:1023–8.
18. Shaw AT, Felip E, Bauer TM, Besse B, Navarro A, Postel-Vinay S, et al. Lorlatinib in non-small-cell lung cancer with ALK or ROS1 rearrangement: an international, multicentre, open-label, single-arm first-in-man phase 1 trial. Lancet Oncol 2017;18:1590–9.
19. Christensen JG, Olson P, Briere T, Wiel C, Bergo MO. Targeting Kras(g12c) -mutant cancer with a mutation-specific inhibitor. J Intern Med 2020;288: 183–91.
20. Ostrem JM, Peters U, Sos ML, Wells JA, Shokat KM. K-Ras(G12C) inhibitors allosterically control GTP affinity and effector interactions. Nature 2013;503: 548–51.
21. Hu Q, Shokat KM. Disease-causing mutations in the G protein galphas subvert the roles of GDP and GTP. Cell 2018;173:1254–64.
22. U.S. Food and Drug Administration. FDA approves first targeted therapy for lung cancer mutation previously considered resistant to drug therapy; 2021. Available from: https://www.fda.gov/news-events/press-announcements/fda-approves-first-targeted-therapy-lung-cancer-mutation-previously-considered-resistant-drug.
23. Hallin J, Engstrom LD, Hargis L, Calinisan A, Aranda R, Briere DM, et al. The KRAS(G12C) inhibitor MRTX849 provides insight toward therapeutic susceptibility of KRAS-mutant cancers in mouse models and patients. Cancer Discov 2020;10:54–71.
24. Prentice RL, Kalbfleisch JD, Peterson AV Jr, Flournoy N, Farewell VT, Breslow NE. The analysis of failure times in the presence of competing risks. Biometrics 1978;34:541–54.
25. Shimizu K, Gupta A, Brastianos PK, Wakimoto H. Anatomy-oriented stereotactic approach to cerebrospinal fluid collection in mice. Brain Res 2022;1774: 147706.
26. Kiyokawa J, Kawamura Y, Ghouse SM, Acar S, Barcin E, Martinez-Quintanilla J, et al. Modification of extracellular matrix enhances oncolytic adenovirus immunotherapy in glioblastoma. Clin Cancer Res 2021;27:889–902.
27. Miller DS, Bauer B, Hartz AM. Modulation of P-glycoprotein at the blood-brain barrier: opportunities to improve central nervous system pharmacotherapy. Pharmacol Rev 2008;60:196–209.
28. Janne PA, Papadopoulos KP, Ou SI, Rybkin I, Johnson M. A phase 1 clinical trial evaluating the pharmacokinetics (PK), safety, and clinical activity of MRTX849, a mutant-selective small molecule KRAS G12C inhibitor, in advanced solid tumors. AACR-NCI-EORTC International Conference on Molecular Targets and Cancer Therapeutics; 2019; Boston, MA.
29. Fell JB, Fischer JP, Baer BR, Blake JF, Bouhana K, Briere DM, et al. Identification of the clinical development candidate MRTX849, a covalent KRAS(G12C) inhibitor for the treatment of cancer. J Med Chem 2020;63:6679–93.
30. Sanchez-Cespedes M, Parrella P, Esteller M, Nomoto S, Trink B, Engles JM, et al. Inactivation of LKB1/STK11 is a common event in adenocarcinomas of the lung. Cancer Res 2002;62:3659–62.
31. Shih DJH, Nayyar N, Bihun I, Dagogo-Jack I, Gill CM, Aquilanti E, et al. Genomic characterization of human brain metastases identifies drivers of metastatic lung adenocarcinoma. Nat Genet 2020;52:371–7.
32. Awad MM, Liu S, Rybkin II, Arbour KC, Dilly J, Zhu VW, et al. Acquired resistance to KRAS(G12C) inhibition in cancer. N Engl J Med 2021;384: 2382–93.
33. Tanaka N, Lin JJ, Li C, Ryan MB, Zhang J, Kiedrowski LA, et al. Clinical acquired resistance to KRAS(G12C) inhibition through a novel KRAS switch-II pocket mutation and polyclonal alterations converging on RAS-MAPK reactivation. Cancer Discov 2021;11:1913–22.